ORIGINAL PAPER

A new method for the determination of particle contact stiffness

M. Paulick · M. Morgeneyer · A. Kwade

Abstract The behaviour of granular material can be predicted numerically with the discrete element method. This method potentially uses material properties to describe the behaviour of a particle and its interactions with other particles or walls. One characteristic property is the particle contact stiffness. The work described herein reviews on one hand shortly different types of stiffness in particle mechanics and on the other hand, with regard to the experimental work, an overview of the newly developed method to examine the contact behaviour between two particles is given. The advantage of this approach is the exclusion of possible equipment deformation and is, thus, only referring to the deformation of two particles in contact. Therefore, especially the deformation of asperities on the particles' surface can be taken into account. A variety of contact experiments on single and two particles were conducted to validate the new method. Glass beads with a particle diameter from $d_p = 0.8$ to 3.0 mm were chosen and a maximum compression force of $F = 80$ N. While only one material type was studied, this work has the broader implication to present a method for determining a material's contact stiffness and its evolution during increasing contact. This study is part of the PARDEM research network: www.pardem.eu.

M. Paulick (✉) · M. Morgeneyer
Université de Technologie de Compiègne,
Compiègne, France
e-mail: maria.paulick@utc.fr

M. Morgeneyer
e-mail: martin.morgeneyer@utc.fr

A. Kwade
Institut für Partikeltechnik, TU Braunschweig,
Brunswick, Germany
e-mail: A.Kwade@tu-braunschweig.de

1 Introduction

Particulate solids are found in a wide range of industries. Their handling is vigorous for functioning process operations since approximately 50 % of the products and at least 75 % of the raw materials in industry are granular matter [1]. It is estimated that about 40 % of industry capacity is wasted due to unknown behaviour of granular material, resulting into insufficient design of unit operations [2]. The design of unit operations relies on estimations of the constitutive behaviour of granular matter which are often based on continuum approaches. But the overall mechanical properties of granular matter are significantly dependent on micro-scale behaviour between interacting particles. Here, the understanding of how particle properties influence the bulk behaviour of a particle assembly is not yet very well established. Nowadays, simulations with the discrete element method (DEM) provide physical knowledge about particle/particle and particle/wall interactions and can contribute to achieve understanding of the macroscopic behaviour of granular matter in diverse industrial applications and nature's phenomena.

One numerical approach was proposed by Cundall and Strack [3], where particle interactions are computed over time through a recurrent application of Newton's second law of motion. A contact model is implemented to describe the force-deformation behaviour of particles in contact. The governing equation in translational direction holds therefore terms for contact, gravity and drag forces, and is given in Eq. (1):

$$m_i \frac{d\vec{v}_i}{dt} = m_i \vec{g} + \vec{F}_d + \left(\vec{F}_n + \vec{F}_n^d \right) \qquad (1)$$

with mass m_i and translational velocity v_i of particle i, g the gravity, F_d the drag force, F_n the governing normal contact force and F_n^d the normal damping force.

Contact models can be classified into three groups which are contact stiffness models, slip models and bonding models [4]. Especially the contact stiffness models relate the contact force to the relative displacement of the particle during an interaction. The approach can be linear, which is less computational intense, or non-linear. For a non-linear model often the Hertz-Mindlin model is applied which will be discussed later. For further information Kruggel-Emden et al. [5] is proposed who review in their work different contact models in accordance to its implementation in DEM code and the reproducibility of real particle behaviour in contact such as elastic or elasto-plastic behaviour.

Depending on the circumstances of the unit operation to be modelled and on the chosen contact model different parameters must be specified before initiating a simulation. These setup parameters are particle properties as well as particle/particle and particle/wall interaction properties. One of these properties is the parameter describing the elasticity of the contact between two particles, the particle contact stiffness.

1.1 Stiffness term in particle mechanics

In general stiffness represents the resistance of a body against deformation caused by a force or moment of torque. It is often expressed relative to the contact area. Thus, stiffness defines the resistance against the necessary force per displacement (Nm^{-1}) to elastically compress a body. In particle mechanics different types of stiffness can be defined and are summarised in Fig. 1. Each stiffness type is referred to a physical scale: At the level smaller than the particle itself, the submicro scale, the particle surface stiffness can be defined. The surface stiffness is examined by local indentation measurements. Particularly attention must be paid to asperities on a particle's surface, since they can influence the reproducibility of measurements due to the establishment of different contact areas which are necessary to calculate the surface stiffness [6,7]. Further information on the measurement of surface stiffnesses can be found elsewhere [8–10,12]. On the micro scale, corresponding to one particle or the size of one particle, the stiffness of a particle itself is determined by single particle compression experiments. Depending on the particle size and desired load different equipment are available such as nano- and micro indentation for forces below 1 N or material testing machines for higher forces [13,14]. As transfer between micro and macro scale the micro-macro bridge, thus, two particles in contact, is considered. The par-
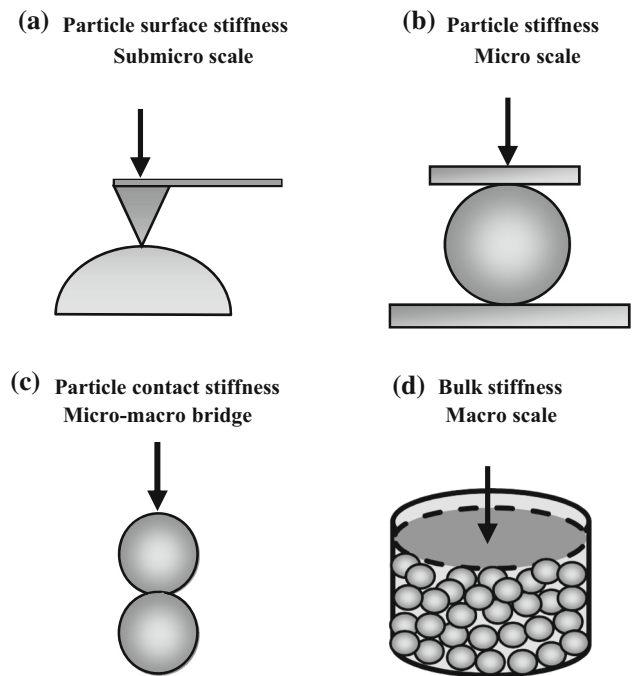

Fig. 1 Overview of stiffness types in particle mechanics

ticle contact stiffness is therefore neither a particle property nor corresponds to a bulk property; it is the result of a superposition of surface roughness and particle stiffness. Different approaches were made to determine a contact stiffness of rather large samples using the contact resonance or ultrasonic method [15,16]. For instance, Shi and Polycarpou [16] used a screw mechanism to fix the samples and further applied the contact resonance method; here, the contact stiffness of flat surfaces were tested. Mullier et al. [17] developed a single-particle friction cell with which particle-particle contact measurements were carried out while the particles are screwed to their holdings. Cole et al. [18] created an experimental system for uniaxial loading of grain pairs until a force of 25 N. On the microscopic level particle-particle experiments were also carried out to determine frictional and adhesive forces [19,20], however, here other approaches like gluing can be applied which less influences the contact behaviour studied here. On the macro scale, referring to multiples particles in contact, the bulk stiffness can be characterised by uniaxial bulk compression experiments [21–24]. The bulk stiffness corresponds to the bulk's resistance to normal compression and, for example, depends amongst others on the coordination number [25].

1.2 Particle contact stiffness

Different theories [26–29] were developed to describe the contact behaviour between two bodies. One of the most common theories is the description of an elastic contact between two spherical bodies offered by Hertz [30]. Hertz assumes

spherical bodies of an elastic isotropic material in frictionless contact. The established stress at contact is described as elliptical distribution in the contact area with a maximum pressure in the centre of the contact area [31,32]. The resulting contact force F_n due to the deformation δ is established as shown by Eq. (2):

$$F_n = \frac{2}{3} E^* \sqrt{R^* \cdot \delta^3} \tag{2}$$

with E^* (Pa) as reduced Young's Modulus, R^* (m) as reduced particle diameter and δ (m) as overlap distance between two particles. The reduced parameters are calculated from material and particle properties of particle 1 and particle 2 according to Eqs. (3) and (4) [32]:

$$E^* = 2 \left(\frac{1 - \nu_1^2}{E_1} + \frac{1 - \nu_2^2}{E_2} \right)^{-1} \tag{3}$$

$$R^* = \left(\frac{1}{R_1} + \frac{1}{R_2} \right)^{-1} \tag{4}$$

with ν = Poisson's Ratio (–), E = Young's modulus (Pa) and R = radius of the particle (m).

The contact stiffness is the numerical derivative at a given load level. According to Hertz the contact stiffness in normal direction between two spherical bodies is then described by Eq. (5):

$$k_n = \frac{dF_n}{d\delta} = E^* \sqrt{R^* \cdot \delta}. \tag{5}$$

In practice, the contact stiffness is often equated with the single particle stiffness measured through single particle compression as shown in Fig. 1b. Therefore, compression tests of single particles have been carried out by a variety of research teams with different compression apparatuses using particle sizes of 1–3 mm and forces up to 35 N as mentioned earlier [33–35]; some of them especially for the characterisation of stiffness [11,36–38].

In DEM simulation the contact stiffness does not only describe the contact between particles, but it is also a crucial parameter influencing the time step of the simulation. Therefore, the particle contact stiffness is often reduced in order to reduce the simulation time [39]. On the other hand different investigations have shown that a reduced contact stiffness, or reduced Young's modulus, can influence the simulation result in an undesirable manner: for instance, in 2007 Moreno-Atanasio et al. [40] showed that in DEM simulation of fluidised beds the fluidisation behaviour of cohesive material can range from particles at rest to fluidisation, depending on the set contact stiffness and surface energy. Also Antony et al. [41] showed that for shear experiments the influence of normal and tangential stiffness on simulation results seems especially important for the characteristic behaviour of assemblies of non-spherical particles. For

example, for confined compression tests, which are especially important in geotechnical and civil engineering, Coetzee et al. [42] identified the high influence of stiffness on the compression behaviour of granules. Similar responses were obtained by Lowery and Zeghal [43] who investigated the influence of stiffness on the resilient behaviour of aggregated materials.

The aim of the work presented here is to understand how the contact stiffness of a particle-particle contact can be experimentally measured by presenting a new method. Attention is drawn to the difference of particle contact stiffness in comparison to single particle stiffness and theoretical Hertzian contact stiffness.

2 Materials and methods

2.1 Materials

Spherical granule soda-lime glass from two different suppliers with different mean particle sizes, 0.8, 1.5 and 3.0 mm, have been chosen and are presented in Fig. 2. Due to the nearly ideally spherical shape it is possible to apply the Hertzian contact theory of spheres [30] for description of elastic deformation behaviour of these granules. A summary of the material properties, including the parameters necessary for the calculation of the particle contact according to Hertz's theory, is given in Tables 1 and 2, respectively.

The surface roughness has been characterised by means of atomic force microscopy, XE-100, Park Systems, on a surface of 30 μm × 30 μm on three different specimens. The topography measurement was carried out with a C-AFM head
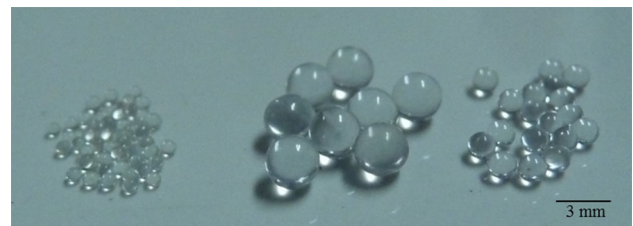

Fig. 2 Image of the granules used in this paper with d_p = 0.8, 1.5, 2.98 mm

Table 1 Mechanical properties of glass beads and steel plate

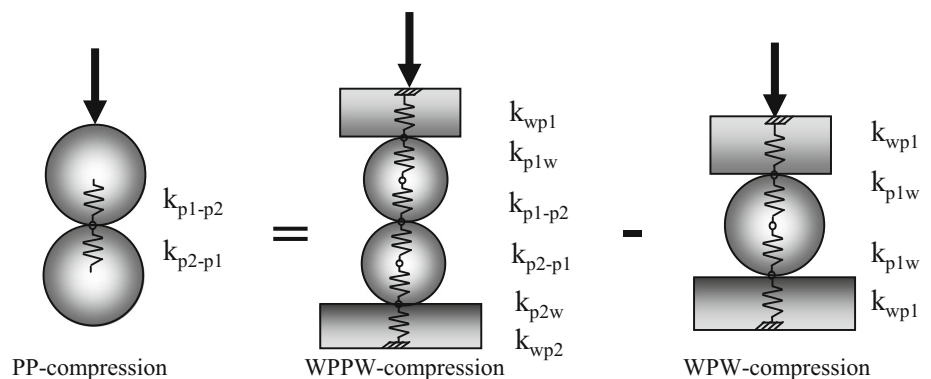| Material	Poisson's ratio ν (–)	E-modulus E (GPa)	Particle radius R (m)
Mechanical properties of the materials			
3.0 mm glass granule	0.22	65	1.5×10^{-3}
1.5 mm glass granule	0.22	65	0.75×10^{-3}
0.8 mm glass granule	0.22	65	0.4×10^{-3}
Steel plate	0.28	200	–

Table 2 Reduced material parameters for the Hertzian contact model after Eq. (4)

Particle	Reduced E-modulus E* (GPa)	Reduced radius R* (m)		
		$d_p = 3.0$ mm	$d_p = 1.5$ mm	$d_p = 0.8$ mm
Parameters for the Hertzian model				
3.0 mm glass spheres	68	0.75×10^{-3}	–	–
1.5 mm glass spheres	68	–	0.375×10^{-3}	–
0.8 mm glass spheres	68	–	–	0.2×10^{-3}
Steel wall	104	1.5×10^{-3}	0.75×10^{-3}	0.4×10^{-3}

Table 3 Measured surface roughness obtained by means of atomic force microscopy

Material	Roughness average R_a (µm)	Root mean square roughness R_q (µm)	Minimum roughness depth R_{Min} (µm)	Maximum roughness depth R_{Max} (µm)
0.8 mm glass spheres	0.155	0.183	−0.552	0.571
1.5 mm glass spheres	0.029	0.038	−0.210	0.160
3.0 mm glass spheres	0.035	0.050	−0.414	0.451

mode and a scan rate of 0.5 Hz. The data editing took then place with the AFM software XEI, where first the surface is straightened with a fit of second order and then the roughness is determined. Here, R_a describes the mean roughness of the surface and R_q corresponds to the root-mean-squared roughness [44]; the minimum and maximum values, R_{Min} and R_{Max}, are presented in Table 3. With Ra = 155 nm, the 0.8 mm glass spheres show the highest average roughness with an extremely high maximum and minimum roughness depth of $R_{Min} = 0.552$ nm and $R_{Max} = 0.571$ nm. The 1.5 and 3.0 mm glass spheres own four times less surface irregularities with $R_{a,1.5mm} = 29$ nm and $R_{a,3.0mm} = 35$ nm. For all particles the R_q-value is close to the R_a-value, indicating a smooth surface with some slightly higher valleys and peaks.

2.2 Method for determining particle contact stiffness

As mentioned in Sect. 1.1 the particle contact stiffness k describes the stiffness at the contact between two particles. However, until now single particle stiffnesses were measured and used as simulation parameters. That is why a new method to directly identify the contact stiffness is introduced. This approach is advantageous since for forces <1 N micro irregularities, such as asperities, can be taken into account. As well as for forces >1 N possible deformation of the measurement equipment, for instance for similar Young's modulus of specimen and apparatus, can be eliminated.

The method is based on a simple mechanical model, considering that each deformation at a contact point in normal direction can be described by a spring stiffness. Therefore, the developing contact stiffness between two particles in contact can be characterized as a serial connection of two springs each with its own stiffness, k_{p1-p2} and k_{p2-p1}, as shown in Fig. 3 on the left side. How this contact stiffness can be experimentally obtained by compression experiments is further explained with the mechanical model of serial connection of contact constellations in the centre and on the right side of Fig. 3. In the centre, the arrangement of two particles between an upper and lower wall is shown; also referred to as wall-particle-particle-wall (WPPW) constellation. The overall established stiffness of this constellation, k_{wppw}, is the summation of six contact stiffness as given in Eq. (6):

Fig. 3 Mechanical model of a serial connection of contact constellation with PP-arrangement (*left*), WPPW-arrangement (*middle*) and WPW-arrangement (*right*) and its stiffness k at each contact
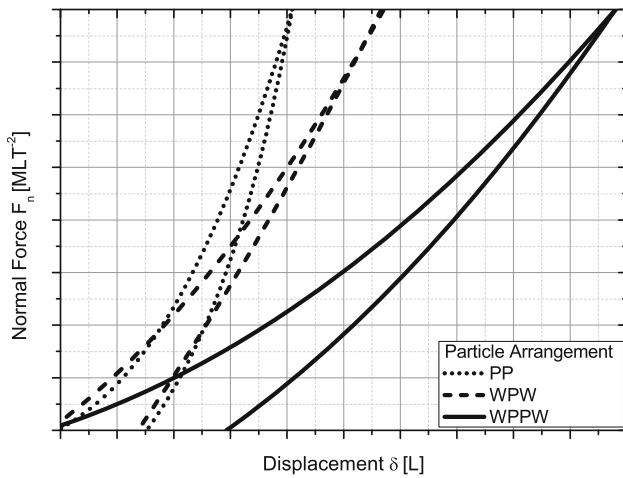
Fig. 4 Scheme of force-displacement curves obtained through WPW- and WPPW-compression and the mathematically resulting PP-compression curve

$$k_{n,WPPW} = \left(\frac{1}{k_{wp1}} + \frac{1}{k_{p1w}} + \frac{1}{k_{p1-p2}} + \frac{1}{k_{p2-p1}} + \frac{1}{k_{p2w}} + \frac{1}{k_{kwp2}} \right)^{-1}. \quad (6)$$

On the right side of Fig. 3 the constellation of the known single particle compression is shown; here referred to as wall-particle-wall (WPW) arrangement. The measurable overall stiffness, k_{wpw}, results from the established contacts and, thus, four stiffnesses as presented in Eq. (7) can be identified:

$$k_{n,WPW} = \left(\frac{1}{k_{wp1}} + \frac{1}{k_{p1w}} + \frac{1}{k_{p1w}} + \frac{1}{k_{wp1}} \right)^{-1}. \quad (7)$$

The influences of upper and lower walls during a compression experiment are eliminated by excluding wall-particle contacts. This exclusion takes place when subtracting the WPW-stiffnesses from the WPPW-stiffnesses as demonstrated in Fig. 3, which leads to the particle-particle (PP) constellation, describing the PP-contact. The mathematically expression is given in Eq. (8):

$$k_{n,PP} = k_{n,WPPW} - k_{n,WPW}$$
$$= \left(\frac{1}{k_{p1-p2}} + \frac{1}{k_{p2-p1}} \right)^{-1} = k_n. \quad (8)$$

Now and in the following the PP-contact stiffness is considered to describe the total overlap of both particles.

Practically, each contact stiffness as shown in Eqs. (6) and (7) cannot be measured to obtain the overall $k_{n,WPW}$ and $k_{n,WPPW}$ stiffnesses, but as stiffness corresponds to the slope of force-displacement data, the overall stiffnesses are obtained through WPW- and WPPW-compression experiments. Figure 4 shows schematically through experiments obtained WPPW- and WPW-force-displacement curves. Knowing at each force level the corresponding displacement, the WPW-displacement is subtracted from the WPPW-displacement, resulting into the data for the PP-force-displacement curve, which is likewise shown in Fig. 4. Now, from all three force-displacement curves for any given load the corresponding stiffness can be derived. However, a displacement controlled measurement is not possible, because for the same displacement much lower forces are needed for the WPPW-constellation and, thus, the WPW-data cannot be subtracted from the WPPW-data.

3 Experiment

3.1 Experimental setup

Based on the proposed method discussed in Sect. 2 it is chosen to compress a single particle as well as two particles with a material testing machine. Figure 5 shows the selected device, Zwick Z010 (Zwick/Roell, Zwick GmbH & Co. KG, Germany), with a closer look at the setup of the WPW- and WPPW-compression. The lower stationary punch is a 4×5 cm^2 steel square and equals the material of the upper 1 cm^2 punch. For the WPPW-compression two particles are placed one above each other in a hollow cylinder made of brass. Three different hollow cylinders were fabricated with a CNC lathe so that the height of the cylinder corresponds to 1.5 times the particle diameter and the inner diameter of the cylinder was chosen to be about 7 % wider than the particle diameter. A lower percentage would have had let to insertion problems for particles with a slightly larger diameter and a higher percentage would allow too much movement of the particles, including shifted top particles towards one side. The exact dimensions are given in This method is especially interesting for contact stiffness measurement of non-spherical particles which could jump away if they are not hindered, for example, by a wall.

Table 4 and a picture is included in Fig. 5 on the right bottom. Wall friction of the hollow cylinder is neglected, since the horizontal dilatation of the particles due to vertical compression plus the particle diameter are minor than the cylinder diameter. This method is especially interesting for contact stiffness measurement of non-spherical particles which could jump away if they are not hindered, for example, by a wall.

Table 4 Dimensions of hollow cylinders for WPPW-compression with a tolerance below 100 μm

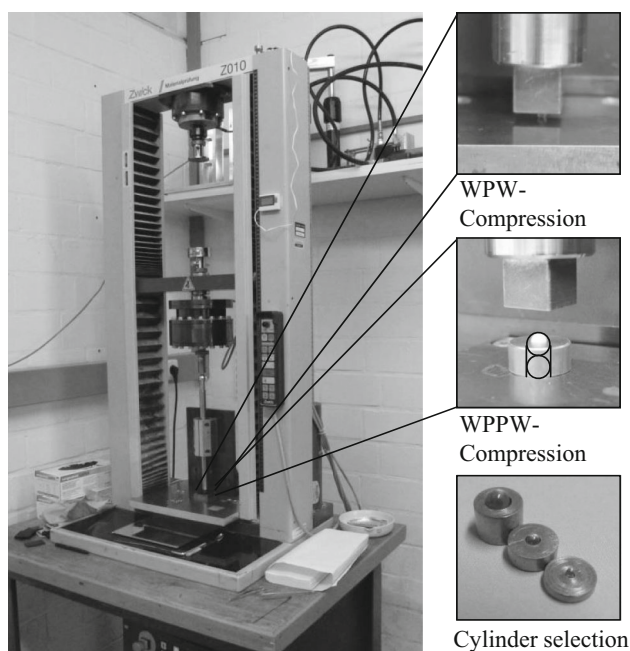|	Particle diameter (m)		
	0.003	0.0015	0.0008
Cylinder size (m)	D = 0.0032	D = 0.0018	D = 0.0011
	H = 0.0042	H = 0.00225	H = 0.0012

Fig. 5 Material testing machine (*left*) and closer look of the WPW-setup with lower and upper plate (*right, top*) and WPPW-setup with the cylinder (*right, middle*) and the cylinder selection for 0.8, 1.5 and 3 mm particles

3.2 Experimental procedure

Experiments are performed for normal compressive loading of one particle and of two particles. In order to examine the loading rate dependency, measurements were carried out at five different punch speeds: 20, 40, 60, 90 and 120 μm/min. A velocity of 90 μm/min gave the best reproducibility and is therefore chosen as loading rate. The experimental system is force-controlled so that the loading stops at a given maximum force which is set to F = 80 N for the following experiments. The sample to be tested is placed unto the lower stationary punch and the upper punch is lowered at a rate of 0.1 mm/min until a first contact is detected. Then the force is set to 0 N and the compression velocity is decreased to v = 90 μm/min. Once the maximum force is attained the upper punch raises immediately, maintaining the velocity, until 0 N contact force is detected.

For the WPPW-compression experiment the first particle is placed inside the hollow cylinder on the lower stationary punch and the second particle is positioned on top of the first one. For both compression types, WPW and WPPW, ten measurements are carried out. Normally, up to 100 measurements are necessary to obtain a standard deviation below 10 %. However, since we apply spherical and non-porous particles, the standard deviations are between 4 and 10 % which is sufficient to validate this new method. Furthermore, to examine the new method cyclic loading of the particles is tested and a 0 N—maximum force repetition is chosen,

resulting into five 80 N–0 N–80 N loading and unloading cycles. Hereby, it cannot be assured, that particles will keep the exact contact point. However, since the cylinder hole is only slightly larger than the particles itself, larger movements can be precluded. The maximum shift of the particles is calculable, while the drawback of adhesive methods, for instance influences through the operator, cannot be determined.

Throughout the experiment the load-displacement curves are registered. Repetitive experiments are performed to determine the range of variation of the contact stiffness. Since the obtained data varies, the mean value for force and displacement are calculated. A polynomial fit of second order is drawn to describe the WPPW- and WPW-displacement at a given force value. With these obtained data sets the loading and unloading curve for the PP-deformation can be determined as described in Sect. 2.

4 Experimental results and discussion

The experiments are carried out as described in the previous section. Figure 6 summarises the experimentally obtained force-displacement curves with normalised contact force for loading and unloading of WPPW- and WPW-compression for all three particle sizes. The equivalent radius R^*_{WPW} for the WPW-contact equals the particle radius. For the WPPW-contact the equivalent radius R^*_{WPPW} takes the particles' radii into account. All applied values are presented in Table 2. Further introduced in Fig. 6 is the polynomial second order description of the graphs and the calculated PP-force-displacement curve for loading which must be determined prior to normalising the contact force.

In the following the determination of the particle contact stiffness is discussed using the example of 3.0 mm glass beads, followed by a discussion on the influence of particle size and of cyclic loading on the particle stiffness value. At the end the experimental data is compared to the theoretical Hertzian approach.

4.1 Determination of particle contact stiffness

With regard to the diagram c in Fig. 6 two areas can be distinguished: For low forces the WPW-force-displacement curve increases faster than the PP-graph. At about 500 $Nm^{-1/2}$ the displacement for the PP-compression rises over that of the WPW-compression. The steeper the slope, the higher is the contact stiffness as shown in Fig. 7. In this figure the evolution of contact stiffness over normalised contact force (with the equivalent radius R^*) for three different cases is presented: First the experimentally measured WPW-stiffness is averaged and shown with its deviation. Further, the polynomial description of WPW-stiffness is plotted, which underestimates the experimentally determined WPW-
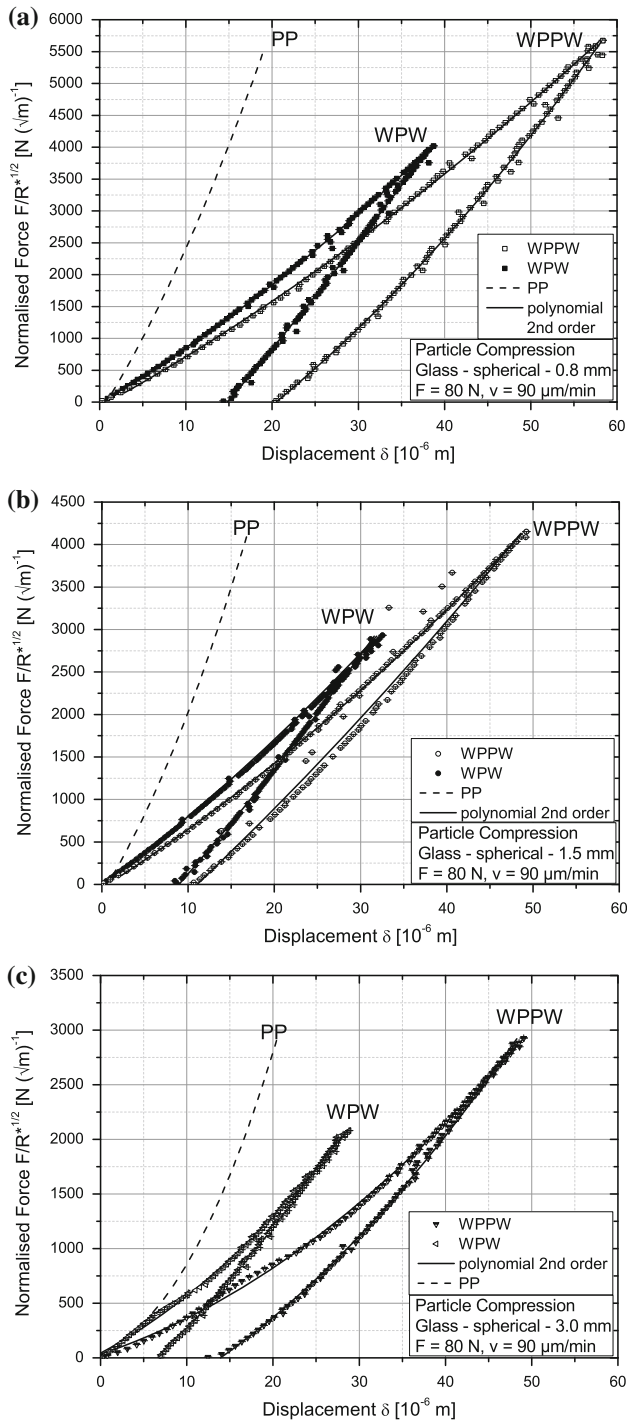
(a)

(b)

(c)

Fig. 6 Averaged load-displacement curves for WPPW- and WPW-compression with polynomial second order description and calculated PP-force-displacement curve for **a** 0.8 mm, **b** 1.5 mm and **c** 3.0 mm glass beads
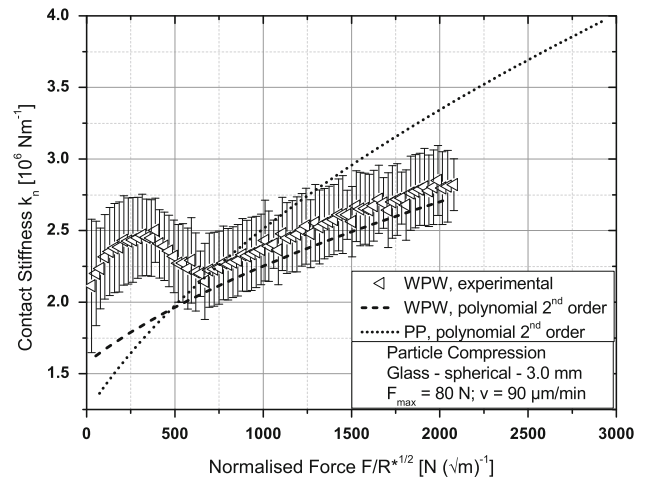

Fig. 7 PP- and WPW-contact stiffness values related to normalised contact force for 3.0 mm glass beads; standard deviation of 10 measurements in average and median below 10 %

ing normalised contact force up to 2,050 $Nm^{-1/2}$. Remarkable is the increase and fall of the WPW-stiffness between 0 and 600 $Nm^{-1/2}$. An explanation of this behaviour is not found for this evolution was not seen for the compression of 0.8 and 1.5 mm glass beads (not shown here). Furthermore, the roughness of the 3.0 mm particles' surface is only slightly higher as for the 1.5 mm glass beads so that a roughness influence should be negligible, however, only the appearance of surface asperities followed by a contact flattening could explain the obtained bend. The evolution of the WPW-stiffness is not well described by the second order polynomial which is imprecise for forces close to 0 N. That is why the bend is not seen for the PP-contact stiffness which increases from 1.36×10^6 Nm^{-1} to 3.96×10^6 Nm^{-1}. Thus, the PP-contact stiffness is for low forces, $F < 500$ $Nm^{-1/2}$; lower than the WPW-stiffness, but rises almost twice as high at maximum force. It seems that at the beginning of a contact the particles' surfaces influence the contact behaviour and therefore the force-displacement behaviour and a varying contact stiffness is obtained. For example, for a particle with a rough surface the contact is not immediately established between two particles' surfaces but between their asperities. Consequently, the PP-force-displacement is lower than the WPW-curve for low forces and, thus, the PP-contact stiffness is lower than the WPW-stiffness. Carpick et al. [45] revealed the influence of asperities on the contact area-load relation established with different indentation tip shapes. It is proven that the possible contact area between two bodies is arbitrative for the contact stiffness which is apparently the case at the initialisation of a particle-particle contact.

4.2 Influence of particle size on particle contact stiffness

In the previous section the utilisation of single particle stiffness versus particle contact stiffness was discussed. Now the
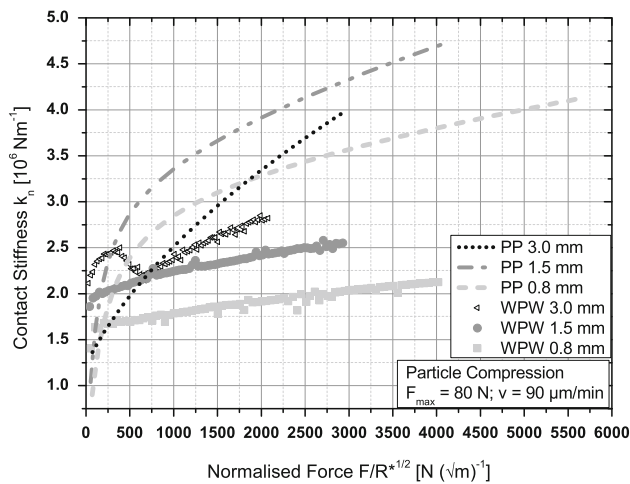
stiffness until approximately 600 $Nm^{-1/2}$, then the polynomial fit approaches the experimental values. Thirdly, the PP-contact stiffness is plotted over the normalised force.

The WPW-stiffness increases from $k_{n,WPW} = 2.15 \times 10^6$ Nm^{-1} to $k_{n,WPW} = 2.85 \times 10^6$ Nm^{-1} during an increas-

Fig. 8 Stiffness values related to normalised force for WPW- and PP-compression of 0.8, 1.5 and 3.0 mm glass beads

influence of particle size is analysed with the new method. For that glass beads with a diameter of 0.8, 1.5 and 3.0 mm, respectively, are examined. The force-displacement curves for all three materials are plotted in Fig. 6. It is shown that the smaller the particle, the higher the deformation of the particle for the same load. The remanent plastic deformation at Force F = 0 N specifies that with regard to the particle size, a stronger flattening of smaller particles takes place. The effect of particle size on stiffness, and thus, that the larger the particle diameter, the higher the stiffness, has been discussed before by Antonyuk et al. [46].

In Fig. 8 the experimentally obtained WPW-stiffnesses for all three particle sizes over normalised normal force as well as the polynomial description for the PP-compression are shown. Apart from the bend in the 3 mm WPW-stiffness graph, larger particles own an increased WPW-stiffness over smaller particles. Very well presented in Fig. 8 is the strong increase of PP-contact stiffness during contact establishment. Therefore, an overestimation of the PP-contact stiffness occurs for low forces when applying the WPW-contact stiffness. Furthermore, it shows that a PP-contact is much stiffer for higher forces than the WPW-constellation since less elastic contacts (e.g. between particle and wall) are taken into account. An influence of surface roughness as presented in Table 3 is not remarkable because of the high chosen contact forces. An influence of surface properties is especially expected for minor forces.

4.3 Influence of multiple contacts on particle contact stiffness

Further investigations demonstrate how the new method can be applied to cyclic loading. Cyclic loading of particles is used to simulate multiple contacts between particles. For that
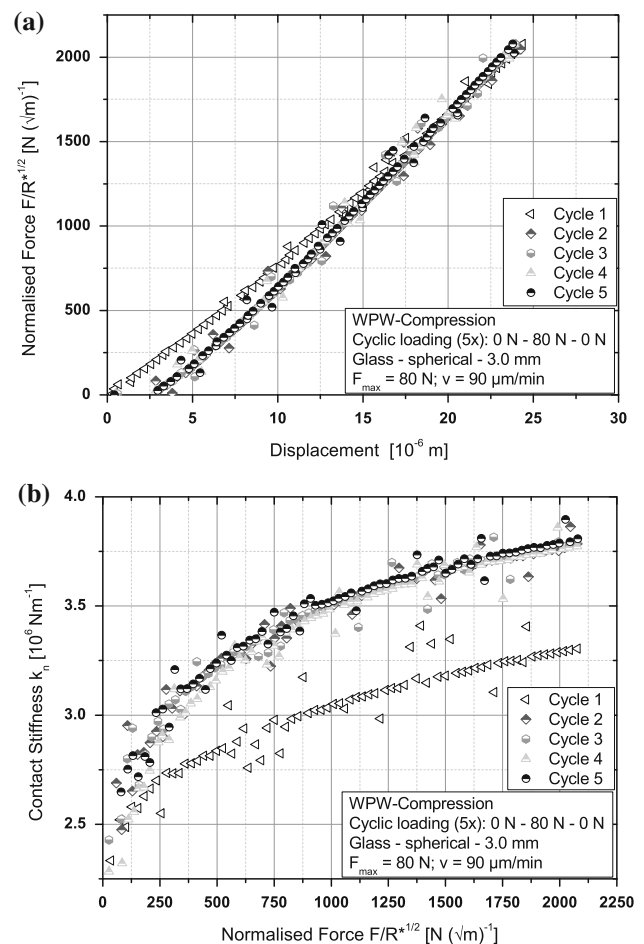

Fig. 9 **a** Five loading-curves for cyclic WPW-compression and **b** corresponding WPW-stiffness values for 3.0 mm glass beads

after each loop the contact force is decreased until F = 0 N is reached, denoting a contact release, followed by a steady increase until the maximum force is reached, which is here set to F_{max} = 80 N. Figure 9a presents experimentally determined loading-curves for WPW-compression of 3 mm glass beads and in Fig. 9b the corresponding WPW-stiffness values in dependence of the normalised contact Force. In both diagrams a remarkable difference between the first and the second cycle is presented while further distinction between cycle two to cycle five is almost not possible. A slightly increase of WPW-stiffness with further loading is noticeable which is in accordance to scientific results obtained by Mader-Arndt et al. [14]. While in their research, carried out in the μN force range, the force-displacement curves are increasing with increasing number of contacts, a further, significant increase might not be possible here due to high forces the particles are exposed to and resulting flattening of the contact areas. Furthermore, Cole et al. [18] found in their grain-pairs experiment, carried out until a force of 10 N, the so-called seating effect, between the initial loading curve and
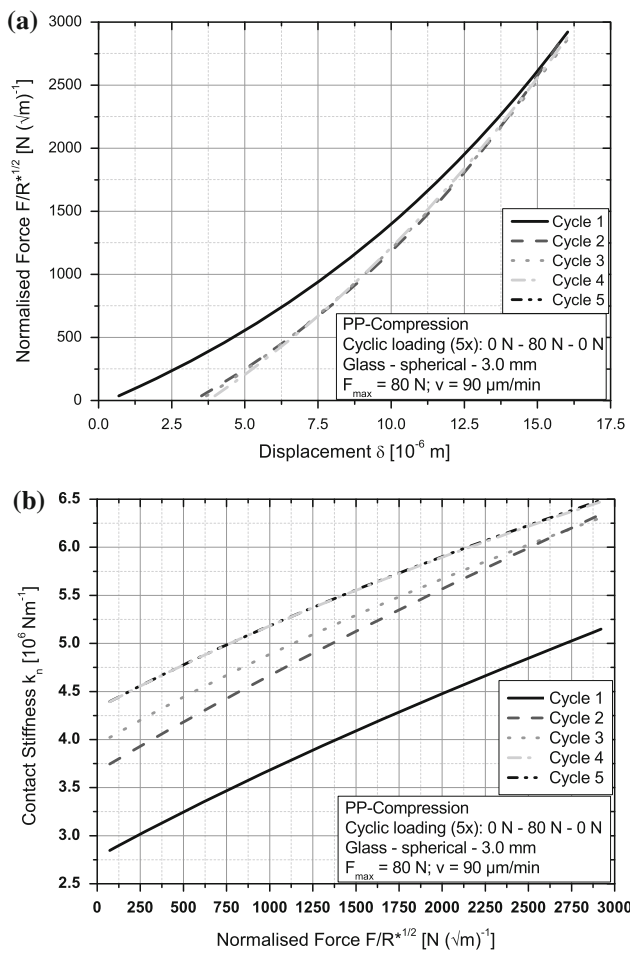
Fig. 10 **a** Five loading-curves for cyclic PP-compression and **b** corresponding PP-contact stiffness values for 3.0 mm glass beads

Fig. 11 Force-displacement curves for **a** WPW-, PP- and Hertzian PP-compression and **b** evolution of stiffness to normalised force for 3.0 mm glass beads

the more similar following loading cycles. The same result was found here, showing a hardening effect due to changes in the particle's structure.

The PP-force displacement and PP-contact stiffness evolution are plotted in Fig. 10a, b respectively. A change of contact point during continuous loading and unloading would lead to similar force-compression curves as obtained for the first cycle. However, as shown in Fig. 10a the second to fifth cycle are similar as previously discussed for the WPW-compression. Therefore, a movement of the particles can be excluded.

The first contact corresponds to a lower contact stiffness than the following contacts, hence, the PP-contact stiffness increases with increase of number of contacts. Furthermore it seems as if a saturation point is reached here as well: An increase of PP-contact stiffness is shown for the first to the fourth contact cycle, but the fifth lies very close to the fourth so that the PP-contact stiffness can be hardly distinguished. This phenomena has been described by Antonyuk et al. [11, 12], which implies that the material started to flow during the
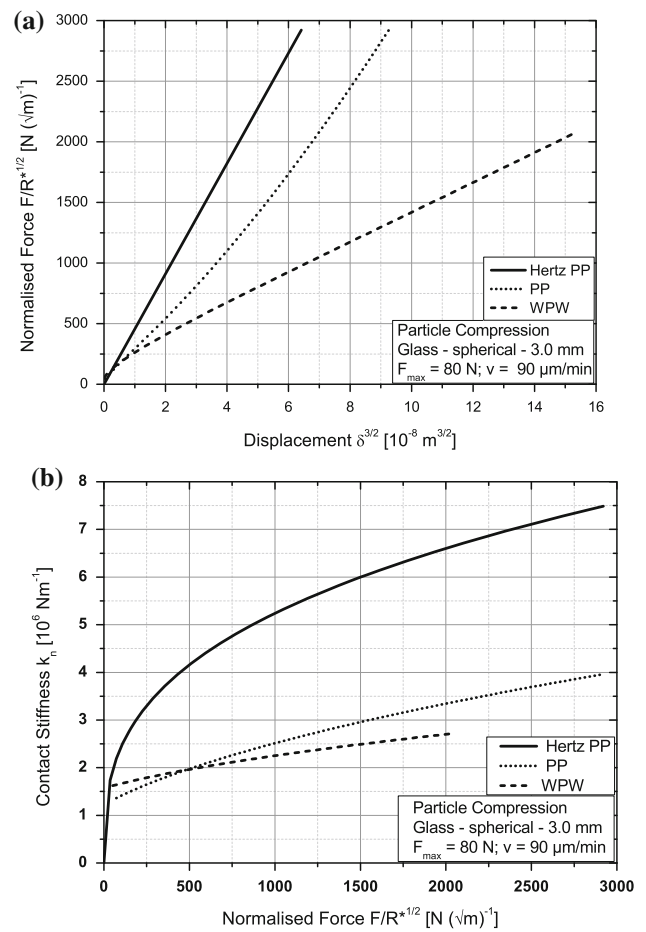
first contact and stays remanent plastically deformed during the following contacts.

A comparison between Figs. 9b and 10b demonstrates very well the difference between a stiffness obtained through WPW- (single particle) and PP-compression. While for the first cycle a WPW-stiffness of $k_{n,WPW} = 2.0 - 3.25 \times 10^{-6}$ Nm^{-1} is attained; the PP-contact stiffness increases more strongly from $k_{n,PP} = 2.8 \times 10^{-6}$ to $k_{n,PP} = 5.1 \times 10^{-6}$ Nm^{-1}. Therefore, the physical response of two particles in contact differs to that from one particle due to surficial changes which are neglected during a WPW-compression.

4.4 Comparison with Hertzian approach

As mentioned before the Hertzian contact model is often used to describe the contact of spherical particles. According to Hertz's theory the particle deformation behaves to the power of 3/2. With Eqs. (2), (3) and (4) and the material properties given in Tables 1 and 2 the Hertzian force-displacement curve and contact stiffness for 3.0 mm glass beads are calculated as presented in Fig. 11.

The Hertzian force-displacement curve is presented in Fig. 11a as straight line as the displacement is normalised to the power of 3/2. As long as the WPW- and PP-force-displacement curves correspond to the straight line, the particle contact is elastic, otherwise they show non-elastic behaviour [32]. It can be seen that elastic deformation of the particles took place for very low forces. For the PP-compression non-elastic deformation begins at about $125\,\mathrm{Nm}^{-1/2}$ which corresponds to 1.5 N normal force. For the WPW-compression the non-elastic deformation starts at about $250\,\mathrm{Nm}^{-1/2}$, which corresponds to 5 N. Elsewhere [38] compression experiments showed as well that for elasto-plastic particles the divergence from the Hertzian curve is below a force of 10 N. Nevertheless, at the beginning of the compression, thus for low forces below 10 N, the PP-deformation is more elastic and a higher deformation is obtained. However, once the plastic deformation for the WPW-constellation starts, a higher deformation than for the contact deformation between two particles is obtained. The micro yield pressure, σ_{Yield} (Pa), is almost identical to the maximal pressure at the centre of contact [47], p_{max} (Pa), and, thus, can be calculated with Eq. (2), the measured deformation at yield point, $\delta_{n,Y}$ (m), and the measured force at yield point, $F_{n,Y}$ (N):

$$\sigma_{Yield} \approx p_{\max} = \frac{3}{2}\frac{F_{n,Y}}{\pi R^* \delta_{n,Y}}. \tag{9}$$

The normal force at yield point for the PP-contact was measured to 6.3 N and the displacement was determined to $2.52\,\mu\mathrm{m}$, therefore a relatively large micro yield pressure of $\sigma_{yield} = 796$ MPa was obtained.

Regarding the obtained stiffness as shown by the diagram in Fig. 11b, the difference between WPW- and PP-contact stiffness is significant. The experimentally obtained PP-stiffness follows the same trend as the theoretically obtained Hertzian stiffness. The difference between both PP-stiffness curves could be due to the fact that the Hertzian curve was calculated with supplier data and should therefore not be taken as a correct but as an appropriate solution. As predicted by the force-deformation curve, a higher WPW-stiffness than PP-stiffness is obtained while being in the elastic deformation range, probably overestimating the stiffness of a contact. With further load the WPW-contact stiffness increases less and shows a more linear behaviour.

5 Conclusions

A simple and straightforward experimental method is developed to determine the contact stiffness of two spherical particles in contact. This experimental method avoids drawbacks as caused through adhesive methods. And contrary to the apparatus as developed by Mullier et al. [17] where particles are fixed through micro-screws, this method can be applied in any compression tester.

Experiments were conducted on two particles, resulting into a wall-particle-particle-wall (WPPW) arrangement and on single particles, resulting into a wall-particle-wall (WPW) arrangement. Subtracting force-displacement curves obtained from both particle arrangements, particle-particle (PP) force-displacement data is obtained which is useful to investigate the influence of asperities or other surface phenomena, such as adhesion, on the PP-contact behaviour.

Theoretically, the optimal stiffness value which can be obtained is that of a PP-contact and is therefore the numerical derivation of the force-displacement curve of two particles in contact. This work shows that the stiffness obtained by a WPW-compression underestimates the stiffness of a PP-contact as obtained with this novel method. One explanation for this underestimation could be a deformation which is not only encountered by the particle itself but also from the device used for the measurement. Furthermore, for forces below 5 N the contact between two 3 mm glass spheres is softer than predicted by the WPW-stiffness. These lower values suggest that there is an influence of particle surfaces on the established contact which should be taken into account when determining the PP-contact stiffness.

Future work includes the application of this new method to lower force ranges as they are applied in atomic force microscopy or contact frictional measurements.

References

1. Nedderman, R.M.: Statics and Kinematics of Granular Materials. Cambridge University Press, Cambridge (2005)
2. Ennis, B.J., Green, J., Davies, R.: The legacy of neglect in the US. Chem. Eng. Prog. **90**(4), 32–43 (1994)
3. Cundall, P.A., Strack, O.D.L.: A discrete numerical model for granular assemblies. Geotechnique **29**, 47–65 (1979)
4. Johnstone, M.W.: Calibration of DEM Models for Granular Materials Using Bulk Physical Tests. Doctor of Philosophy, The University of Edinburgh (2010)
5. Kruggel-Emden, H., Simsek, E., Rickelt, S., Wirtz, S., Scherer, V.: Review and extension of normal force models for the discrete element method. Powder Technol. **171**(3), 157–173 (2007). doi:10.1016/j.powtec.2006.10.004
6. Mann, A.B., Pethica, J.B.: The role of atomic size asperities in the mechanical deformation of nanocontacts. Appl. Phys. Lett. **69**(7), 907–909 (1996)
7. Bobji, M.S., Biswas, S.K.: Deconvolution of hardness from data obtained from nanoindentation of rough surfaces. J. Mater. Res. **14**(6), 2259–2268 (1999)
8. Fischer-Cripps, A.C.: Introduction to Contact Mechanics. Springer, New York (2000)

9. Pharr, G.M., Oliver, W.C., Brotzen, F.R.: On the generality of the relationship among contact stiffness, contact area, and elastic modulus during indentation. J. Mater. Res. **7**(3), 613–617 (1992)

10. Li, X., Bhushan, B.: A review of nanoindentation continuous stiffness measurement technique and its applications. Mater. Charact. **48**(1), 11–36 (2002). doi:10.1016/s1044-5803(02)00192-4

11. Antonyuk, S., Palis, S., Heinrich, S.: Breakage behaviour of agglomerates and crystals by static loading and impact. Powder Technol. **206**(1–2), 88–98 (2011). doi:10.1016/j.powtec.2010.02.025

12. Müller, P., Antonyuk, S., Tomas, J.: Simulation of the compression and impact behavior of zeolith 4A granules [Simulation des Druck- und Stoßvorgangs von Zeolith 4A-Granulaten]. Chemie Ingenieur Technik **83**(5), 643–651 (2011). doi:10.1002/cite.201000212

13. Cavarretta, I., Coop, M., O'Sullivan, C.: The influence of particle characteristics on the behaviour of coarse grained soils. Geotechnique **60**(6), 413–423 (2010). doi:10.1680/geot.2010.60.6.413

14. Mader-Arndt, K., Kutelova, Z., Fuchs, R., Meyer, J., Staedler, T., Hintz, W., Tomas, J.: Single particle contact versus particle packing behavior: model based analysis of chemically modified glass particles. Granul. Matter, 1–17 (2014). doi:10.1007/s10035-013-0478-9

15. Robinson, A.M., Drinkwater, B.W., Dwyer-Joyce, R.S., Payne, J.F.B.: Measurement of the stiffness of joints in graphite brick assembly. Proc. Inst. Mech. Eng. Part C J. Mech. Eng. Sci. **215**(2), 167–178 (2001). doi:10.1243/0954406011520599

16. Shi, X., Polycarpou, A.A.: Measurement and modeling of normal contact stiffness and contact damping at the meso scale. J. Vib. Acoust. Trans. ASME **127**(1), 52–60 (2005). doi:10.1115/1.1857920

17. Mullier, M., Tüzün, U., Walton, O.R.: A single-particle friction cell for measuring contact frictional properties of granular materials. Powder Technol. **65**(1–3), 61–74 (1991)

18. Cole, D.M., Peters, J.F.: A physically based approach to granular media mechanics: grain-scale experiments, initial results and implications to numerical modeling. Granul. Matter. **9**(5), 309–321 (2007)

19. Heim, L.O., Blum, J., Preuss, M., Butt, H.J.: Adhesion and friction forces between spherical micrometer-sized particles. Phys. Rev. Lett. **83**(16), 3328–3331 (1999)

20. Daeinabi, K., Korayem, M.H.: Indentation analysis of nano-particle using nano-contact mechanics models during nano-manipulation based on atomic force microscopy. J. Nanopart. Res. **13**(3), 1075–1091 (2011). doi:10.1007/s11051-010-0096-y

21. Cohen, M.L.: Calculation of bulk moduli of diamond and zinc-blende solids. Phys. Rev. B **32**(12), 7988–7991 (1985). doi:10.1103/PhysRevB.32.7988

22. Gaith, M.S., Alhayek, I.: The measurement of overall elastic stiffness and bulk modulus in anisotropic materials: semiconductors. In: Lake Buena Vista, FL 2010. 2009 ASME International Mechanical Engineering Congress and Exposition, IMECE2009, pp. 29–34

23. Kruyt, N.P., Agnolin, I., Luding, S., Rothenburg, L.: Micromechanical study of elastic moduli of loose granular materials. J. Mech. Phys. Solids **58**(9), 1286–1301 (2010)

24. Walton, K.: The effective elastic moduli of a random packing of spheres. J. Mech. Phys. Solids **35**(2), 213–226 (1987)

25. Lätzel, M., Luding, S., Herrmann, H.J.: Macroscopic material properties from quasi-static, microscopic simulations of a two-dimensional shear-cell. Granul. Matter. **2**(3), 123–135 (2000)

26. Derjaguin, B.V., Muller, V.M., Toporov, Y.P.: Effect of contact deformations on the adhesion of particles. J. Colloid Interface Sci. **53**(2), 314–326 (1975)

27. Walton, O.R., Braun, R.L.: Viscosity, granular-temperature, and stress calculations for shearing assemblies of inelastic, frictional disks. J. Rheol. **30**(5), 949–980 (1986)

28. Thornton, C., Ning, Z.: A theoretical model for the stick/bounce behaviour of adhesive, elastic-plastic spheres. Powder Technol. **99**(2), 154–162 (1998)

29. Brilliantov, N.V., Spahn, F., Hertzsch, J.M., Pöschel, T.: Model for collisions in granular gases. Phys. Rev. E **53**(5 SUPPL. B), 5382–5392 (1996)

30. Hertz, H.: Über die Berührung fester elastischer Körper. J. Für die reine Angew Math. **92**, 156–171 (1881)

31. Johnson, K.L.: Contact Mech. Cambridge University Press, Cambridge (1985)

32. Tomas, J.: Adhesion of ultrafine particles—a micromechanical approach. Chem. Eng. Sci. **62**(7), 1997–2010 (2007). doi:10.1016/j.ces.2006.12.055

33. Yap, S.F., Adams, M.J., Seville, J.P.K., Zhang, Z.: Single and bulk compression of pharmaceutical excipients: evaluation of mechanical properties. Powder Technol. **185**(1), 1–10 (2008)

34. Samimi, A., Hassanpour, A., Ghadiri, M.: Single and bulk compressions of soft granules: experimental study and DEM evaluation. Chem. Eng. Sci. **60**(14), 3993–4004 (2005). doi:10.1016/j.ces.2005.02.036

35. Yoshida, M., Ogiso, H., Nakano, S., Akedo, J.: Compression test system for a single submicrometer particle. Rev. Sci. Instrum. **76**(9), 093905 (2005)

36. Romeis, S., Paul, J., Ziener, M., Peukert, W.: A novel apparatus for in situ compression of submicron structures and particles in a high resolution SEM. Rev. Sci. Instrum. **83**(9) (2012). doi:10.1063/1.4749256

37. Paul, J., Romeis, S., Tomas, J., Peukert, W.: A review of models for single particle compression and their application to silica microspheres. Adv. Powder Technol. **25**(1), 136–153 (2014). doi:10.1016/j.apt.2013.09.009

38. Russell, A., Müller, P., Tomas, J.: Multiple compression of moist spherical elastic-plastic zeolite 4A granules. Chem. Eng. Technol. **36**(7), 1240–1248 (2013). doi:10.1002/ceat.201300109

39. Bierwisch, C.S.: Numerical Simulations of Granular Flow and Filling. Albert-Ludwigs-Universität Freiburg, Freiburg im Breisgau (2009)

40. Moreno-Atanasio, R., Xu, B.H., Ghadiri, M.: Computer simulation of the effect of contact stiffness and adhesion on the fluidization behaviour of powders. Chem. Eng. Sci. **62**(1–2), 184–194 (2007). doi:10.1016/j.ces.2006.08.036

41. Antony, S.J., Moreno-Atanasio, R., Hassanpour, A.: Influence of contact stiffnesses on the micromechanical characteristics of dense particulate systems subjected to shearing. Appl. Phys. Lett. **89**(21) (2006). doi:10.1063/1.2396894

42. Coetzee, C.J., Els, D.N.J., Dymond, G.F.: Discrete element parameter calibration and the modelling of dragline bucket filling. J. Terramech. **47**(1), 33–44 (2010). doi:10.1016/j.jterra.2009.03.003

43. Lowery, M., Zeghal, M.: Effects of particle and mix characteristics on performance of some granular materials. In: CANCAM 2003, Calgary, Alberta, June 1–6, 2003, pp. 302–303 (2003)

44. Park Systems Corporation: XE-100 User's Manual, vol. Version 1.0. (2002)

45. Carpick, R.W., Ogletree, D.F., Salmeron, M.: Lateral stiffness: a new nanomechanical measurement for the determination of shear strengths with friction force microscopy. Appl. Phys. Lett. **70**(12), 1548–1550 (1997)

46. Antonyuk, S., Heinrich, S., Tomas, J., Deen, N.G., Van Buijtenen, M.S., Kuipers, J.A.M.: Energy absorption during compression and impact of dry elastic-plastic spherical granules. Granul. Matter. **12**(1), 15–47 (2010). doi:10.1007/s10035-009-0161-3

47. Antonyuk, S.: Deformations- und Bruchverhalten von kugelförmigen Granulaten bei Druck- und Stoßbeanspruchung. Docupoint-Verlag, Magdeburg (2006)